EUROPEAN ORGANISATION FOR PARTICLE PHYSICS

CERN-PPE/94-42
10 March 1994

Measurement of the $\tau^- \to \mathrm{h}^-\pi^0\nu_\tau$ and $\tau^- \to \mathrm{h}^- \geq 2\pi^0\nu_\tau$ Branching Ratios

The OPAL Collaboration

Abstract

The branching ratios of the $\tau^- \to \mathrm{h}^-\pi^0\nu_\tau$ and $\tau^- \to \mathrm{h}^- \geq 2\pi^0\nu_\tau$ decays (where h^- is either a π^- or K^-) are measured using the OPAL detector at LEP. The two branching ratios are simultaneously measured using separate selection criteria and are found to be

$$\begin{aligned} \mathrm{B}_{\mathrm{h}^-\pi^0} &= (26.25 \pm 0.36 \pm 0.52)\% \\ \mathrm{B}_{\mathrm{h}^-\geq 2\pi^0} &= (9.89 \pm 0.34 \pm 0.55)\% \\ \mathrm{B}_{\mathrm{h}^-\pi^0} + \mathrm{B}_{\mathrm{h}^-\geq 2\pi^0} &= (36.14 \pm 0.33 \pm 0.58)\% \end{aligned}$$

where the first error is statistical and the second is systematic.

(Submitted to Physics Letters B)

The OPAL Collaboration

R. Akers[16], G. Alexander[23], J. Allison[16], K.J. Anderson[9], S. Arcelli[2], S. Asai[24], A. Astbury[28], D. Axen[29], G. Azuelos[18,a], A.H. Ball[17], R.J. Barlow[16], S. Barnett[16], R. Bartoldus[3], J.R. Batley[5], G. Beaudoin[18], A. Beck[23], G.A. Beck[13], J. Becker[10], C. Beeston[16], T. Behnke[27], K.W. Bell[20], G. Bella[23], P. Bentkowski[18], P. Berlich[10], S. Bethke[32], O. Biebel[3], I.J. Bloodworth[1], P. Bock[11], B. Boden[3], H.M. Bosch[11], M. Boutemeur[18], P. Bright-Thomas[25], R.M. Brown[20], A. Buijs[8], H.J. Burckhart[8], C. Burgard[27], P. Capiluppi[2], R.K. Carnegie[6], A.A. Carter[13], J.R. Carter[5], C.Y. Chang[17], C. Charlesworth[6], D.G. Charlton[8], S.L. Chu[4], P.E.L. Clarke[15], J.C. Clayton[1], I. Cohen[23], J.E. Conboy[15], M. Cooper[22], M. Coupland[14], M. Cuffiani[2], S. Dado[22], C. Dallapiccola[17], G.M. Dallavalle[2], C. Darling[31], S. De Jong[13], L.A. del Pozo[5], H. Deng[17], M. Dittmar[4], M.S. Dixit[7], E. do Couto e Silva[12], J.E. Duboscq[8], E. Duchovni[26], G. Duckeck[8], I.P. Duerdoth[16], D.J.P. Dumas[6], P.A. Elcombe[5], P.G. Estabrooks[6], E. Etzion[23], H.G. Evans[9], F. Fabbri[2], B. Fabbro[21], M. Fierro[2], M. Fincke-Keeler[28], H.M. Fischer[3], R. Folman[26], D.G. Fong[17], M. Foucher[17], A. Fürtjes[8], A. Gaidot[21], J.W. Gary[4], J. Gascon[18], N.I. Geddes[20], C. Geich-Gimbel[3], S.W. Gensler[9], F.X. Gentit[21], T. Geralis[20], G. Giacomelli[2], P. Giacomelli[4], R. Giacomelli[2], V. Gibson[5], W.R. Gibson[13], J.D. Gillies[20], J. Goldberg[22], D.M. Gingrich[30,a], M.J. Goodrick[5], W. Gorn[4], C. Grandi[2], F.C. Grant[5], J. Hagemann[27], G.G. Hanson[12], M. Hansroul[8], C.K. Hargrove[7], P.F. Harrison[13], J. Hart[8], P.A. Hart[9], P.M. Hattersley[1], M. Hauschild[8], C.M. Hawkes[8], E. Heflin[4], R.J. Hemingway[6], G. Herten[10], R.D. Heuer[8], J.C. Hill[5], S.J. Hillier[8], T. Hilse[10], D.A. Hinshaw[18], P.R. Hobson[25], D. Hochman[26], R.J. Homer[1], A.K. Honma[28,a], R.E. Hughes-Jones[16], R. Humbert[10], P. Igo-Kemenes[11], H. Ihssen[11], D.C. Imrie[25], A. Jawahery[17], P.W. Jeffreys[20], H. Jeremie[18], M. Jimack[1], M. Jones[6], R.W.L. Jones[8], P. Jovanovic[1], C. Jui[4], D. Karlen[6], K. Kawagoe[24], T. Kawamoto[24], R.K. Keeler[28], R.G. Kellogg[17], B.W. Kennedy[15], J. King[13], S. Kluth[5], T. Kobayashi[24], M. Kobel[10], D.S. Koetke[8], T.P. Kokott[3], S. Komamiya[24], R. Kowalewski[8], R. Howard[29], J. von Krogh[11], J. Kroll[9], P. Kyberd[13], G.D. Lafferty[16], H. Lafoux[8], R. Lahmann[17], J. Lauber[8], J.G. Layter[4], P. Leblanc[18], P. Le Du[21], A.M. Lee[31], E. Lefebvre[18], M.H. Lehto[15], D. Lellouch[26], C. Leroy[18], J. Letts[4], L. Levinson[26], Z. Li[12], S.L. Lloyd[13], F.K. Loebinger[16], G.D. Long[17], B. Lorazo[18], M.J. Losty[7], X.C. Lou[8], J. Ludwig[10], A. Luig[10], M. Mannelli[8], S. Marcellini[2], C. Markus[3], A.J. Martin[13], J.P. Martin[18], T. Mashimo[24], P. Mättig[3], U. Maur[3], J. McKenna[29], T.J. McMahon[1], J.R. McNutt[25], F. Meijers[8], F.S. Merritt[9], H. Mes[7], A. Michelini[8], R.P. Middleton[20], G. Mikenberg[26], J. Mildenberger[6], D.J. Miller[15], R. Mir[12], W. Mohr[10], C. Moisan[18], A. Montanari[2], T. Mori[24], M. Morii[24], U. Müller[3], B. Nellen[3], H.H. Nguyen[9], S.W. O'Neale[1], F.G. Oakham[7], F. Odorici[2], H.O. Ogren[12], C.J. Oram[28,a], M.J. Oreglia[9], S. Orito[24], J.P. Pansart[21], P. Paschievici[26], G.N. Patrick[20], M.J. Pearce[1], P. Pfister[10], J.E. Pilcher[9], J. Pinfold[30], D. Pitman[28], D.E. Plane[8], P. Poffenberger[28], B. Poli[2], T.W. Pritchard[13], H. Przysiezniak[18], G. Quast[27], M.W. Redmond[8], D.L. Rees[8], G.E. Richards[16], M. Rison[5], S.A. Robins[13], D. Robinson[5], A. Rollnik[3], J.M. Roney[28], E. Ros[8], S. Rossberg[10], A.M. Rossi[2], M. Rosvick[28], P. Routenburg[30], K. Runge[10], O. Runolfsson[8], D.R. Rust[12], M. Sasaki[24], C. Sbarra[2], A.D. Schaile[26], O. Schaile[10], F. Scharf[3], P. Scharff-Hansen[8], P. Schenk[4], B. Schmitt[3], H. von der Schmitt[11], M. Schröder[12], H.C. Schultz-Coulon[10], P. Schütz[3], M. Schulz[8], C. Schwick[27], J. Schwiening[3], W.G. Scott[20], M. Settles[12], T.G. Shears[5], B.C. Shen[4], C.H. Shepherd-Themistocleous[7], P. Sherwood[15], G.P. Siroli[2], A. Skillman[16], A. Skuja[17], A.M. Smith[8], T.J. Smith[28], G.A. Snow[17], R. Sobie[28], R.W. Springer[17], M. Sproston[20], A. Stahl[3], C. Stegmann[10], K. Stephens[16], J. Steuerer[28],

R. Ströhmer[11], D. Strom[19], H. Takeda[24], S. Tarem[8], M. Tecchio[9], P. Teixeira-Dias[11], N. Tesch[3], M.A. Thomson[15], E. Torrente-Lujan[22], S. Towers[6], N.J. Tresilian[16], T. Tsukamoto[24], M.F. Turner[8], D. Van den plas[18], R. Van Kooten[12], G.J. VanDalen[4], G. Vasseur[21], M. Vincter[28], A. Wagner[27], D.L. Wagner[9], C. Wahl[10], C.P. Ward[5], D.R. Ward[5], J.J. Ward[15], P.M. Watkins[1], A.T. Watson[1], N.K. Watson[7], P. Weber[6], P.S. Wells[8], N. Wermes[3], B. Wilkens[10], G.W. Wilson[4], J.A. Wilson[1], V-H. Winterer[10], T. Wlodek[26], G. Wolf[26], S. Wotton[11], T.R. Wyatt[16], R. Yaari[26], A. Yeaman[13], G. Yekutieli[26], M. Yurko[18], W. Zeuner[8], G.T. Zorn[17].

[1]School of Physics and Space Research, University of Birmingham, Birmingham B15 2TT, UK
[2]Dipartimento di Fisica dell' Università di Bologna and INFN, I-40126 Bologna, Italy
[3]Physikalisches Institut, Universität Bonn, D-53115 Bonn, Germany
[4]Department of Physics, University of California, Riverside CA 92521, USA
[5]Cavendish Laboratory, Cambridge CB3 0HE, UK
[6]Carleton University, Department of Physics, Colonel By Drive, Ottawa, Ontario K1S 5B6, Canada
[7]Centre for Research in Particle Physics, Carleton University, Ottawa, Ontario K1S 5B6, Canada
[8]CERN, European Organisation for Particle Physics, CH-1211 Geneva 23, Switzerland
[9]Enrico Fermi Institute and Department of Physics, University of Chicago, Chicago IL 60637, USA
[10]Fakultät für Physik, Albert Ludwigs Universität, D-79104 Freiburg, Germany
[11]Physikalisches Institut, Universität Heidelberg, D-69120 Heidelberg, Germany
[12]Indiana University, Department of Physics, Swain Hall West 117, Bloomington IN 47405, USA
[13]Queen Mary and Westfield College, University of London, London E1 4NS, UK
[14]Birkbeck College, London WC1E 7HV, UK
[15]University College London, London WC1E 6BT, UK
[16]Department of Physics, Schuster Laboratory, The University, Manchester M13 9PL, UK
[17]Department of Physics, University of Maryland, College Park, MD 20742, USA
[18]Laboratoire de Physique Nucléaire, Université de Montréal, Montréal, Quebec H3C 3J7, Canada
[19]University of Oregon, Department of Physics, Eugene OR 97403, USA
[20]Rutherford Appleton Laboratory, Chilton, Didcot, Oxfordshire OX11 0QX, UK
[21]DAPNIA/SPP, Saclay, F-91191 Gif-sur-Yvette, France
[22]Department of Physics, Technion-Israel Institute of Technology, Haifa 32000, Israel
[23]Department of Physics and Astronomy, Tel Aviv University, Tel Aviv 69978, Israel
[24]International Centre for Elementary Particle Physics and Department of Physics, University of Tokyo, Tokyo 113, and Kobe University, Kobe 657, Japan
[25]Brunel University, Uxbridge, Middlesex UB8 3PH, UK
[26]Particle Physics Department, Weizmann Institute of Science, Rehovot 76100, Israel
[27]Universität Hamburg/DESY, II Institut für Experimental Physik, Notkestrasse 85, D-22607 Hamburg, Germany
[28]University of Victoria, Department of Physics, P O Box 3055, Victoria BC V8W 3P6, Canada
[29]University of British Columbia, Department of Physics, Vancouver BC V6T 1Z1, Canada
[30]University of Alberta, Department of Physics, Edmonton AB T6G 2J1, Canada
[31]Duke University, Dept of Physics, Durham, NC 27708-0305, USA

[32]Universität Aachen, III Physikalisches Institut, Sommerfeldstrasse 26-28, D-52056 Aachen, Germany

[a]Also at TRIUMF, Vancouver, Canada V6T 2A3

1 Introduction

Compilations of τ branching ratio measurements suggest an inconsistency when the inclusive single-charged-particle or one-prong decay mode is compared with the sum of all the exclusive one-prong decay modes [1]. This inconsistency between the inclusive and exclusive branching ratios is not, however, supported by ALEPH [2] and CELLO [3]. Most measurements of the $\tau^- \to \mathrm{e}^-\bar{\nu}_\mathrm{e}\nu_\tau$, $\tau^- \to \mu^-\bar{\nu}_\mu\nu_\tau$ and $\tau^- \to \mathrm{h}^-\nu_\tau$ (where h^- is either a π^- or K^-) branching ratios are consistent with each other. However the branching ratios of the τ to hadrons accompanied by π^0's are less well known and additional measurements of these branching ratios may help resolve some of the current ambiguity. This paper reports on a measurement of the branching ratios of the $\tau^- \to \mathrm{h}^-\pi^0\nu_\tau$ and $\tau^- \to \mathrm{h}^- \geq 2\pi^0\nu_\tau$ decays using the OPAL detector at LEP.

The τ leptons from $\mathrm{Z}^0 \to \tau^+\tau^-$ decay are highly energetic and the subsequent τ decay products are collimated along the τ direction of motion. Two different $\mathrm{h}^-\pi^0$ selections that strive to separate the decay products are presented. One uses a shower shape technique where the reconstructed energy depositions in the lead-glass blocks are compared with reference distributions. The other $\mathrm{h}^-\pi^0$ selection and the $\mathrm{h}^- \geq 2\pi^0$ selection use a fine clustering algorithm.

Both $\mathrm{h}^-\pi^0$ selections produce samples with the background dominated by $\mathrm{h}^- \geq 2\pi^0$ decays. Similarly, the $\mathrm{h}^- \geq 2\pi^0$ sample has a background dominated by $\mathrm{h}^-\pi^0$ decays. The number of $\mathrm{h}^-\pi^0$ and $\mathrm{h}^- \geq 2\pi^0$ candidates can be expressed in terms of the two branching ratios. The two branching ratios can be simultaneously derived using these expressions, eliminating the need to use any previous measurement of them. The branching ratios for other τ decays do need to be included, but their influence on the final results is small.

The $\tau^- \to \mathrm{h}^-\pi^0\nu_\tau$ branching ratio measured here includes the $\tau^- \to \pi^-\pi^0\nu_\tau$ and $\tau^- \to \mathrm{K}^-\pi^0\nu_\tau$ channels. The $\tau^- \to \mathrm{h}^- \geq 2\pi^0\nu_\tau$ branching ratio also includes the $\tau^- \to \mathrm{h}^-\mathrm{K}^0_S\nu_\tau \to \mathrm{h}^-2\pi^0\nu_\tau$ decay. The $\tau^- \to \mathrm{h}^- \geq 2\pi^0\nu_\tau$ branching ratio includes contributions from the $\tau^- \to \pi^-2\pi^0\nu_\tau$ and $\tau^- \to \pi^-3\pi^0\nu_\tau$ channels as the $\mathrm{h}^- \geq 2\pi^0$ selection criteria do not distinguish between the two channels. The $\tau^- \to \mathrm{h}^-4\pi^0\nu_\tau$ decay or the other τ decays involving photons, such as the $\tau^- \to \pi^-\omega\nu_\tau$ and $\tau^- \to \eta\pi^-\pi^0\nu_\tau$ decays, were not modelled, however their influence on the branching ratios is discussed.

2 OPAL Detector

The results presented here are based on data taken during the 1991 and 1992 runs with the OPAL detector at LEP. Over 90% of the data were recorded at the peak of the Z^0 resonance with the remainder taken at center-of-mass energies within ± 3 GeV of the peak. Details of the OPAL detector can be found in reference [4]. Only a brief account of some relevant features for the present analysis is given here.

The tracking of charged particles is performed with a central detector that contains three drift chambers: a precision inner vertex chamber, a large volume jet chamber and specialized chambers at the outer radius of the jet chamber which improve track position measurements in the z-direction. The coordinate system is defined so that z is the coordinate along the e^- beam axis, r is the coordinate normal to the beam axis, ϕ is the azimuthal angle and θ is the polar angle with respect to the z-axis. The tracking chambers are enclosed by a solenoidal magnet coil providing an axial field of 0.435 T. The average angular resolution of the combined tracking system is about 0.2 mrad in ϕ and better than 10 mrad in θ. The OPAL central detector also includes a silicon microvertex detector.

Electromagnetic energy is measured by a detector composed of lead-glass blocks located

outside the magnet coil, divided into a barrel ($|\cos\theta| < 0.82$) and two endcaps ($0.81 < |\cos\theta| < 0.98$). Each block subtends approximately 40×40 mrad^2. The depth of material to the back of the calorimeter is about 25 radiation lengths. The electromagnetic calorimeter has a time-of-flight detector and presampler in front of it. The time-of-flight detector consists of 160 scintillator bars covering the barrel region and the presampler consists of limited streamer tubes in the barrel region and thin multiwire chambers for the endcaps.

Outside the electromagnetic calorimeter, the OPAL detector is instrumented with a hadron calorimeter, constructed from alternating layers of iron slabs and limited streamer tubes. The thickness of the material is typically eight interaction lengths. Outside the hadron calorimeter is the muon chamber system, composed of four layers of drift chambers for $|\cos\theta| < 0.68$ and four layers of limited streamer tubes for $0.60 < |\cos\theta| < 0.98$.

3 Selection of $\tau^+\tau^-$ Candidates

The procedure used to select $Z^0 \to \tau^+\tau^-$ events is similar to that described in previous OPAL publications [5, 6]. The candidate event must contain 2-6 good charged tracks and less than 10 clusters in the lead-glass calorimeter. A good charged track must have $p_\perp > 100$ MeV, $|d_0| < 2$ cm and $|z_0| < 75$ cm, where $p_\perp$ is the transverse momentum relative to the beam axis, $|d_0|$ is the distance of closest approach of the track to the beam axis and $|z_0|$ is the displacement along the beam axis from the nominal interaction point at the point of closest approach to the beam. The track must also have at least 20 measured space points in the main jet chamber, and at least one point within 75 cm of the beam axis. A cluster in the barrel lead-glass calorimeter must have a minimum energy of 100 MeV, whereas a cluster in the endcap must have a minimum energy of 200 MeV and contain at least two lead-glass blocks, no one of which may contribute more than 99% to the cluster's energy.

The distinctive signature of a $\tau^+\tau^-$ event is two back-to-back jets with typically one to three charged particles, often accompanied by neutral hadrons or photons. Since the decay products are collimated, it is convenient to treat each τ decay as a jet, as defined in ref. [7], where charged tracks and clusters in the lead-glass electromagnetic calorimeter are assigned to cones of half-angle 35°. A $\tau^+\tau^-$ candidate must contain exactly two jets, each with at least one charged track and with a total track and cluster energy that exceeds 1% of the beam energy. Backgrounds due to two-photon processes and events with radiation are removed by requiring the acolinearity between the two jets to be less than 15°. A fiducial requirement is imposed on the directions of the τ jets to avoid regions of non-uniform response in the lead-glass calorimeter. The average value of $|\cos\theta|$ for the two charged jets must satisfy $\overline{|\cos\theta|} < 0.68$.

There are four main backgrounds. The first background is from $e^+e^- \to e^+e^-$ events, which can be identified by the presence of two high-momentum, back-to-back charged particles with the full center-of-mass energy ($E_{\rm CM}$) deposited in the lead-glass electromagnetic calorimeter. This background can be reduced by requiring $\tau^+\tau^-$ candidates to satisfy either $E_{\rm cluster} \leq 0.8\, E_{\rm CM}$ or $E_{\rm cluster} + 0.3 E_{\rm track} \leq E_{\rm CM}$, where $E_{\rm cluster}$ is the total energy in the lead-glass calorimeter and $E_{\rm track}$ is the total energy of the charged tracks in the event. Hermeticity of the calorimeter ensures reliable identification of $e^+e^- \to e^+e^-\,\gamma$ (and $e^+e^- \to \mu^+\mu^-\gamma$) events.

The second background is from $e^+e^- \to \mu^+\mu^-$ events, which can also be identified by the presence of two high-momentum, back-to-back charged particles but with very little energy deposited in the lead-glass electromagnetic calorimeter. Events are removed if they pass the muon pair selection described in ref. [5]. This selection requires that a track in each jet give a signal consistent with that for a muon and that the scalar sum of the charged track momenta

Background	Contamination(%)
$e^+e^- \to q\bar{q}$	0.42 ± 0.18
$e^+e^- \to e^+e^-$	0.22 ± 0.08
$e^+e^- \to \mu^+\mu^-$	0.91 ± 0.46
$e^+e^- \to e^+e^-\ e^+e^-$	0.09 ± 0.02
$e^+e^- \to e^+e^-\ \mu^+\mu^-$	0.07 ± 0.02
Total	1.71 ± 0.50

Table 1: Estimated background contamination in the $\tau^+\tau^-$ candidate events. The errors include both statistical and systematic uncertainties.

plus the energy of the most energetic lead-glass cluster be greater than $0.6E_{\rm CM}$.

A third background to $e^+e^- \to \tau^+\tau^-$ events comes from $e^+e^- \to q\bar{q}$ (multihadronic) events. This background is less significant at LEP than at lower-energy experiments because the particle multiplicity in $e^+e^- \to q\bar{q}$ events increases with $E_{\rm CM}$, while for $\tau^+\tau^-$ events it remains constant.

Finally, a fourth background comes from two-photon $e^+e^- \to (e^+e^-)X$ events where the final-state electron and positron escape undetected at low angles and the system X is misidentified as a $\tau^+\tau^-$ event. The contribution to the background is small because they lack the enhancement to the cross-section from the Z^0 resonance and because the visible energy (the sum of the charged track and lead-glass cluster energies) of the two-photon system is in general much smaller than that from a $\tau^+\tau^-$ event. An event is rejected if the sum of visible energies of the jets is less than 3% of $E_{\rm CM}$. Further, if the total visible energy is less than 20% of $E_{\rm CM}$, the event is rejected if the missing transverse momenta, calculated separately for charged tracks and for lead-glass clusters, are both less than 2 GeV/c.

Other potential backgrounds arising from cosmic rays and single-beam interactions are suppressed with simple requirements on the time-of-flight detector and on the location of the primary event vertex.

These selection criteria were applied to all the data collected during 1991 and 1992 to give a sample of approximately 27,000 $\tau^+\tau^-$ candidate events. Monte Carlo studies of the $e^+e^- \to e^+e^-$ [8], $e^+e^- \to \mu^+\mu^-$ [9], $e^+e^- \to q\bar{q}$ [10] and $e^+e^- \to (e^+e^-)X$ [11] channels are used to estimate the residual background, as given in Table 1. The total background is $(1.71 \pm 0.50)\%$.

4 $h^-\pi^0$ Selection

The standard OPAL electromagnetic clustering algorithm used in the $\tau^+\tau^-$ preselection was designed for identifying jets in an e^+e^- environment. The clusters were not limited in size nor was the algorithm optimized for distinguishing individual particles. Two alternative approaches were developed with the purpose of improving our ability to distinguish individual particles in τ decays. This was motivated partly by the fact that the $\tau^- \to \rho^-\nu_\tau$ decay is most sensitive to the τ polarization when the π^- and π^0 are extremely close to each other [13]. The measurement of the branching ratio is less sensitive to this but benefits from the increased statistics.

4.1 Selection I

The $h^-\pi^0$ selection I uses reference profiles of the lateral distribution of energy in electron and pion showers in the lead-glass calorimeter to identify hadronic and electromagnetic clusters. Reference shower profiles were obtained using Monte Carlo [12] and cross-checked with electron and pion control samples. The reference profiles predict the fraction of energy in each of the eight blocks surrounding the center block of a candidate cluster. The fraction of energy in a particular block depends on the initial location of the shower within the center block and, for hadrons, on the amount of energy in the hadronic calorimeter.

This selection requires each candidate jet to have exactly one charged track. The track trajectory is extrapolated to the lead-glass calorimeter where it is associated to a particular block. All of the energy in the associated block as well as the predicted energy in its adjacent blocks, based on the hadronic shower profiles, is assigned to the track. The energy associated to the track is then removed from the jet.

Two photon candidates are constructed from the remaining energy. The first photon candidate is assumed to enter the most energetic block and its energy spread to the adjacent blocks is estimated in the same way as the track but using the electromagnetic shower profiles. The energy associated to this photon is removed from the jet and this procedure is repeated in order to identify the second photon candidate from the remaining energy. Initially the location of the photons are assumed to be at the center of their most energetic block. The next step in the algorithm allows the positions of the photons to vary within a discrete grid in their most energetic block. The configuration chosen has the least residual energy (the energy not accounted for by hadronic or photon showers). The final step in the algorithm recalculates the direction of each photon if the reference profile overestimates the energy deposited in any of the surrounding blocks. The direction is calculated using the block coordinates weighted by their partial contribution to the photon energy.

Having identified a jet with a track and two photon candidates, the two photons must have a mass, $M_{\gamma\gamma}$, that is consistent with a π^0, $M_{\gamma\gamma} < 0.3$ GeV, and the mass of the jet, M_{jet}, must satisfy $M_{jet} > 0.6$ GeV. The mass of the two photons and the mass of the jet are plotted in Figure 1. The Monte Carlo is in reasonable agreement with the data when the OPAL τ branching ratios are used.

Further background suppression is obtained by requiring that $|y| \leq 1$, where y is defined by

$$y = \frac{(2E_{\mathrm{h}\pi^0}/E_{\mathrm{beam}} - 1)m_\tau^2 - m_{\mathrm{h}\pi^0}^2}{\beta_\tau(m_\tau^2 - m_{\mathrm{h}\pi^0}^2)}$$

where $E_{\mathrm{h}\pi^0}$ is the energy of the $h^-\pi^0$ system; E_{beam} is the beam energy; and $m_{\mathrm{h}\pi^0}$ is the mass of the $h^-\pi^0$ system. For $h^-\pi^0$ decays, $y = \cos\theta^*$, where $\cos\theta^*$ is defined as the angle of the $h^-\pi^0$ system relative to the τ direction of motion in the τ center-of-mass frame. Decays that are incorrectly identified as $h^-\pi^0$ candidates can give non-physical values for $\cos\theta^*$ and are rejected. The sensitivity of the final results to the $M_{\gamma\gamma}$, M_{jet} and y cuts have been examined over a wide range and are within the quoted systematic errors.

4.2 Selection II

The $h^-\pi^0$ selection II and the $h^- \geq 2\pi^0$ selection use a fine clustering algorithm for identifying particles ($\pi^\pm$, γ or unresolved π^0) in τ decays. This contrasts with the $h^-\pi^0$ selection I where discrete clusters are not a requirement, instead the shape of the energy deposition in the lead-glass calorimeter is deconvoluted into individual particles.

Electromagnetic showers have a lateral size roughly equal to the size of a lead-glass block. Rather than allow the size of cluster to be unrestricted in the number of blocks, it is limited to a maximum size of 2×2 blocks in θ and ϕ. Clusters adjacent to other clusters may have fewer blocks. Both electron data samples and Monte Carlo show that on average 99% of the energy of an electron deposited in the lead-glass calorimeter is contained in a 2×2 cluster.

Hadronic showers have a larger variation in the amount of energy deposited ranging from those particles that leave little energy in the lead-glass blocks to those that start showering early and leave all their energy in the lead-glass. The 2×2 cluster size was optimized for detecting electromagnetic showers, however pion data samples show that on average 95% of the energy that a charged pion deposits in the lead-glass calorimeter is contained within the cluster. Tracks are matched to 2×2 clusters using a χ^2-type significance parameter in θ and ϕ that is weighted by the error in the track position at the lead-glass blocks and in the uncertainty of the cluster centroid. The χ^2 matching parameter and an E/p cut (E is the cluster energy and p is the track momentum) can test if a γ or π^0 overlaps the hadronic shower. The $\mathrm{h}^-\pi^0$ selection II and $\mathrm{h}^- \geq 2\pi^0$ selection use slightly different values, as discussed below. For both $\mathrm{h}^-\pi^0$ selections, the kinematic quantities are calculated using the information from the charged track and the unassociated clusters.

This $\mathrm{h}^-\pi^0$ selection requires each candidate jet to have exactly one charged track with the scaled momentum, $x \equiv p/E_{\mathrm{beam}}$, required to satisfy $x > 0.05$, where p is the charged track momentum and E_{beam} is the beam energy. Further, the track direction at the collision point is required to be within 300 mrad of the original jet direction. Clusters are considered associated to a track if both the polar and azimuthal components of the χ^2, χ^2_θ and χ^2_ϕ respectively, satisfy $\chi^2_\theta < 8$ and $\chi^2_\phi < 8$. Jets that have a γ or π^0 overlapping the track or jets from $\tau^- \to \mathrm{e}^-\bar{\nu}_\mathrm{e}\nu_\tau$ decay are reduced substantially by requiring that the energy, E, of the cluster associated to the track satisfy $E/p < 0.9$. The candidate jet is required to have either one or two clusters not associated to the track with at least 1.4 GeV of energy per cluster and within 300 mrad of the jet axis.

The mass of the jet, M_{jet}, is required to be between 0.5 GeV and 2.0 GeV. The requirement that $M_{\mathrm{jet}} > 0.5$ GeV reduces the background from radiative decays and $\tau^- \to \mathrm{h}^-\nu_\tau$ decays when the hadron showers early in the magnet coil and produces an additional cluster in the lead-glass calorimeter. However, eliminating this requirement would not significantly alter the final result. The jet mass for $\mathrm{h}^-\pi^0$ decays is plotted in Figure 2(a). If the jet contains two neutral clusters then their mass, $M_{\gamma\gamma}$, must be consistent with a π^0 ($M_{\gamma\gamma} < 0.28$ GeV). The mass $M_{\gamma\gamma}$ for $\mathrm{h}^-\pi^0$ decays is plotted in Figure 3(a). With the high energy threshold on individual clusters, only about 10% of the π^0's are reconstructed from two clusters. Consequently the final results are almost insensitive to the $M_{\gamma\gamma} < 0.28$ GeV requirement.

5 $\mathrm{h}^- \geq 2\pi^0$ Selection

The $\mathrm{h}^- \geq 2\pi^0$ selection uses the same clustering algorithm described in the $\mathrm{h}^-\pi^0$ selection II. It requires that each candidate jet have exactly one charged track with scaled momentum $x \geq 0.05$ lying within 500 mrad of the jet direction. Clusters are considered associated to a track if both $\chi^2_\theta < 16$ and $\chi^2_\phi < 16$. The clusters that are not associated to the track are required to have $E > 0.7$ GeV and to be within 500 mrad of the jet direction.

The $\mathrm{h}^- \geq 2\pi^0$ selection uses a more general π^0 identification than employed in the $\mathrm{h}^-\pi^0$ selection. The $\mathrm{h}^-\pi^0$ selection is tighter since it has a higher potential background from other τ decays. The identification of π^0's in the jet proceeds in three steps. The first step identifies all

the pairs of 2×2 clusters that form a π^0 candidate defined as having $0.07 < M_{\gamma\gamma} < 0.23$ GeV and $E_{\gamma\gamma} > 2.6$ GeV, where $M_{\gamma\gamma}$ is the mass and $E_{\gamma\gamma}$ is the energy of the two cluster system. The combination of clusters that gives the maximum number of π^0's in the jet is chosen, and if there is further ambiguity, the combination that gives the highest energy π^0 is chosen. The next step is to look at the remaining clusters and identify them as π^0's if their energy, E, satisfies $E > 2.6$ GeV. Clusters that are neither associated to a track nor form a π^0 candidate are ignored. Finally, the cluster associated to the track is considered a π^0 if $E/p > 1.2$ and $E > 2.6$ GeV. Although the E/p distribution for an isolated charged hadron is rarely greater than 1.0, the higher threshold of $E/p > 1.2$ reduces potential background from electrons.

The π^0 can only be reconstructed from two clusters when its energy is below approximately 10 GeV. Above that energy the two photons are too close to be resolved in the lead-glass calorimeter using this clustering algorithm. To demonstrate that π^0's are observed with this algorithm, jets with one track and two clusters that are not associated to the track have been selected. The mass of the two clusters was plotted in Figure 3(b) if it satisfied $0.07 < M_{\gamma\gamma} < 1.0$ GeV and $E_{\gamma\gamma} > 2.6$ GeV (similar to the requirements given above except that the upper threshold on $M_{\gamma\gamma}$ was raised to 1.0 GeV). The Monte Carlo is in good agreement with the data when OPAL τ branching ratios are used. The background under the π^0 peak comes from τ decays accompanied by radiative photons or from a spurious cluster appearing due to the showering of the charged pion in the magnet coil located in front of the lead-glass calorimeter. The events with $M_{\gamma\gamma} > 0.23$ GeV would normally be classified as either a jet with one π^0 (one cluster being a π^0 candidate and the other cluster with too little energy) or a jet with two π^0's (both clusters being π^0 candidates). Some of the $h^-\pi^0$ decays that appear in the region $M_{\gamma\gamma} > 0.23$ GeV occur when the two clusters from a real π^0 are so close that the angular resolution and consequently the mass resolution is poor. Approximately 25% of the π^0's in the $h^- \geq 2\pi^0$ selection are reconstructed from two clusters and the sensitivity of the final results to the $M_{\gamma\gamma}$ cut is well within the systematic errors presented below.

Jets with two or more identified π^0's are considered $h^- \geq 2\pi^0$ candidates. The mass of the jet, $M_{\rm jet}$, is calculated using the track and π^0's in the jet. The π^0's used in the calculation of $M_{\rm jet}$ use the π^0 mass, rather than the reconstructed mass. The jet mass for $h^- \geq 2\pi^0$ candidates is plotted in Figure 2(b). The jet mass is required to satisfy $M_{\rm jet} < 2.0$ GeV.

6 Branching Ratio Calculation

Both of the $h^-\pi^0$ selections have high efficiency for selecting $h^-\pi^0$ decays with the $h^- \geq 2\pi^0$ decays being the largest background and the other τ decay modes being relatively small. Similarly, the $h^- \geq 2\pi^0$ selection has a high efficiency for selecting $h^- \geq 2\pi^0$ decays with the $h^-\pi^0$ decays being the largest background.

Each selection yields an equation in terms of the efficiencies for selecting a particular channel, the branching ratio of that channel and the fraction of decays selected from the $\tau^+\tau^-$ sample. The two equations can be written as

$$\epsilon_{11}B_1 \; + \epsilon_{12}B_2 \; + \; \sum_{j=3}^{n} \epsilon_{1j}B_j = \; \frac{N_1}{N_\tau} \frac{(1 \; - \; f_1^{non-\tau})}{(1 \; - \; f^{non-\tau})}$$

$$\epsilon_{21}B_1 \; + \epsilon_{22}B_2 \; + \; \sum_{j=3}^{n} \epsilon_{2j}B_j = \; \frac{N_2}{N_\tau} \frac{(1 \; - \; f_2^{non-\tau})}{(1 \; - \; f^{non-\tau})}$$

where the subscript 1 is used to indicate the $h^-\pi^0$ channel and the subscript 2 is used to indicate the $h^- \geq 2\pi^0$ channel. The terms B_1 and B_2 are the branching ratios in the preselected sample. The term ϵ_{ij} is defined to be the efficiency for selecting the j-th channel using the i-th channel selection and is determined from Monte Carlo. The branching ratios B_j, $j \geq 3$, are taken from other sources, as described below. In addition, N_i is the number of decays which pass the i-th selection requirements and N_τ is the number of decays passing the τ decay selection requirements. The $f_1^{non-\tau}$ and $f_2^{non-\tau}$ terms are the non-τ backgrounds in the $h^-\pi^0$ and $h^- \geq 2\pi^0$ samples. The term $f^{non-\tau}$ is the non-τ background in the $\tau^+\tau^-$ sample.

The efficiencies for selecting $h^-\pi^0$ and $h^- \geq 2\pi^0$ decays and the background in the selected samples are determined by Monte Carlo simulations [9]. The Monte Carlo models most τ decay modes including all hadronic decays with four pions and some with five pions in the final state. The hadronic decay modes with two or three hadrons proceed only through the ρ, a_1 or K^* resonances. Four and five hadron modes are calculated only for pions with a phase space calculation. No modelling of τ decays with the η or ω resonances in the decay chain is done. In general, the selection efficiencies are independent of the branching ratios used in the Monte Carlo. However, as the charged hadron can be a π^- or K^-, the efficiencies are calculated as an average of the channels weighted by their respective branching ratios. In addition, the decay of the τ through the K^* resonance leads to four different final states: $K^-\pi^0$, $\pi^-K^0_L$, $\pi^-2\pi^0$ and $\pi^-\pi^+\pi^-$. For a given K^* branching ratio, the fraction of decays in each of the four final states is calculated using isospin symmetry arguments and the measured K^0_S branching ratio.

The equations can be solved for the branching ratios for the $\tau^- \to h^-\pi^0\nu_\tau$ and $\tau^- \to h^- \geq 2\pi^0\nu_\tau$ decay modes if the branching ratios of the other τ decay modes are known. The low efficiency for selecting the other τ decay modes means the $\tau^- \to h^-\pi^0\nu_\tau$ and $\tau^- \to h^- \geq 2\pi^0\nu_\tau$ branching ratios will depend weakly on these branching ratios. As mentioned, the solution of the equations yields branching ratios in the preselected sample. As a result, a correction factor must be applied to these branching ratios to correct the slight bias introduced into the $\tau^+\tau^-$ sample due to the $\tau^+\tau^-$ selection criteria. Monte Carlo simulation indicates that the branching ratios B_1 and B_2 should be divided by 1.0148 ± 0.0067 and 1.0152 ± 0.0072 to obtain the unbiased branching ratios.

7 Results

A total of 8713 out of 56744 jets were identified with the $h^-\pi^0$ selection I, while 10480 jets using the $h^-\pi^0$ selection II and 1688 jets using the $h^- \geq 2\pi^0$ selection were selected out of 54706 jets. The $h^-\pi^0$ selection I has different detector operational status requirements so the total number of τ jets is slightly different. The samples are not statistically independent. The $h^-\pi^0$ selections have 5575 decays in common. The number of decays in common between the $h^- \geq 2\pi^0$ and $h^-\pi^0$ selections is 389 for $h^-\pi^0$ selection I and 67 for $h^-\pi^0$ selection II, respectively.

The efficiencies for selecting particular τ decay modes out of the $\tau^+\tau^-$ sample are listed in Table 2. The error quoted for each efficiency comes entirely from Monte Carlo statistics. The efficiency for selecting $\tau^- \to h^-\pi^0\nu_\tau$ decays is an average of the efficiencies for selecting $\tau^- \to \pi^-\pi^0\nu_\tau$ or $\tau^- \to K^-\pi^0\nu_\tau$ decays weighted by their relative branching ratios. Similarly, the efficiency for selecting $\tau^- \to h^- \geq 2\pi^0\nu_\tau$ decays is based on an average of the efficiencies for selecting $\tau^- \to \pi^-2\pi^0\nu_\tau$, $\tau^- \to \pi^-3\pi^0\nu_\tau$ or $\tau^- \to \pi^-K^0_S\nu_\tau \to \pi^-2\pi^0\nu_\tau$ decays weighted by their relative branching ratios. The efficiencies for these decays and the branching ratios assumed in the calculation of the $h^-\pi^0$ and $h^- \geq 2\pi^0$ efficiencies are given in Table 3. The dependence of the branching ratios on these assumptions will be discussed in the section describing the

Table 2: Selection Efficiencies

Channel	$h^-\pi^0$ Selection I (%)	$h^-\pi^0$ Selection II (%)	$h^- \geq 2\pi^0$ Selection (%)
$h^-\pi^0\ \nu$[1]	46.97 ± 0.16	57.19 ± 0.18	2.76 ± 0.06
$h^- \geq 2\pi^0\ \nu$[2]	22.29 ± 0.20	29.65 ± 0.25	23.16 ± 0.23
$e^-\nu\nu$	0.93 ± 0.04	0.59 ± 0.03	0.07 ± 0.01
$\mu^-\nu\nu$	0.67 ± 0.03	1.09 ± 0.05	0.00 ± 0.00
$h^-\nu$	4.15 ± 0.04	6.72 ± 0.13	0.22 ± 0.03
$K^{*-}\nu \to \pi^- K^0\nu$[3]	9.97 ± 0.43	13.50 ± 0.62	1.31 ± 0.21
$h^-h^+h^- \geq 0\pi^0\nu$	0.11 ± 0.01	0.16 ± 0.02	0.11 ± 0.02

[1] Includes $K^{*-} \to K^\pm\pi^0$

[2] Includes $K^{*-} \to \pi^\pm K^0_S \to \pi^\pm 2\pi^0$

[3] Excludes $K^{*-} \to K^-\pi^0$ and $K^{*-} \to \pi^\pm K^0_S \to \pi^\pm 2\pi^0$

systematic errors.

The background from τ decays other than $h^-\pi^0$ and $h^- \geq 2\pi^0$ decays is estimated to be (4.96±0.14)% , (6.99±0.22)% and (2.20±0.17)% for the $h^-\pi^0$ I, $h^-\pi^0$ II and $h^- \geq 2\pi^0$ selections, respectively (see Table 4). The errors quoted arise from the uncertainty in the selection efficiency and the uncertainty in the branching ratio. The branching ratios used to estimate the background are $B_{e^-\nu\nu} = (17.93 \pm 0.26)\%$, $B_{\mu^-\nu\nu} = (17.58 \pm 0.27)\%$, $B_{h^-\nu} = (12.7 \pm 0.4)\%$, $B_{\pi^- K^0_L\nu} + B_{\pi^-(K^0_S \to \pi^-\pi^+)\nu} = (0.80 \pm 0.12)\%$ and $B_{h^-h^+h^-(\geq 0\pi^0)\nu} = (14.06 \pm 0.25)\%$, which correspond to the "fit" values given in the Particle Data Group summary [1]. There is negligible background in either $h^-\pi^0$ sample from non-τ sources. The background from $e^+e^- \to q\bar{q}$ events in the $h^- \geq 2\pi^0$ sample is estimated to be $(0.46 \pm 0.19)\%$.

One set of branching ratios is determined using the $h^-\pi^0$ selection I with the $h^- \geq 2\pi^0$ selection. A second set of branching ratios is determined using the $h^-\pi^0$ selection II with the $h^- \geq 2\pi^0$ selection. The results are presented in Table 5. The two sets are found to be in excellent agreement.

7.1 Systematic Errors

The systematic uncertainties are given in Table 6. The upper table gives the systematic errors for the branching ratios obtained using the $h^-\pi^0$ I and $h^- \geq 2\pi^0$ selections while the lower table gives the systematic errors for the branching ratios obtained using the $h^-\pi^0$ II and $h^- \geq 2\pi^0$ selections. Both tables also give the systematic error on the sum of the two branching ratios. The sum of the branching ratios is calculated by adding the two branching ratios. The systematic error on the sum of the branching ratios is evaluated independently as the systematic errors for the $h^-\pi^0$ and $h^- \geq 2\pi^0$ branching ratios are correlated. Some of the individual systematic errors are asymmetric, so that the total errors given at the bottom may not equal the quadratic sum of errors in each column.

The systematic errors are presented in two parts in Table 6. The first part gives the errors on the aspects of the analysis such as the modelling of photon conversions, the effect of the $x = p/E_{beam}$ requirement, other tracking requirements and the uncertainty in the overall energy scale. The second part gives the errors on the backgrounds in the sample. The non-τ background, the background from other τ channels, and the influence of the $\pi^-3\pi^0$, K^* and

Table 3: $h^-\pi^0$ and $h^- \geq 2\pi^0$ Efficiencies

$h^-\pi^0$ Efficiency

Channel	$h^-\pi^0$ Selection I (%)	$h^-\pi^0$ Selection II (%)	Branching Ratio (%)
$\pi^-\pi^0$	47.2 ± 0.2	57.5 ± 0.2	26.00
$K^-\pi^0$	36.3 ± 1.0	43.3 ± 1.2	0.47

$h^- \geq 2\pi^0$ Efficiency

Channel	$h^- \geq 2\pi^0$ Selection (%)	Branching Ratio (%)
$\pi^-2\pi^0$	23.0 ± 0.3	8.60
$\pi^-3\pi^0$	26.0 ± 0.7	1.30
$\pi^-K^0_S \to \pi^-2\pi^0$	10.7 ± 1.3	0.15

Table 4: Background Fraction

Channel	$h^-\pi^0$ Selection I (%)	$h^-\pi^0$ Selection II (%)	$h^- \geq 2\pi^0$ Selection (%)
$e^\pm\nu\nu$	0.91± 0.05	0.57± 0.03	0.42± 0.07
$\mu^\pm\nu\nu$	0.65± 0.03	1.04± 0.05	0.01± 0.01
$h^\pm\nu$	2.88± 0.10	4.66± 0.17	0.93± 0.11
$K^{*-}\nu \to \pi^\pm K^0_L\nu$	0.09± 0.01	0.13± 0.02	0.50± 0.08
$h^-h^+h^- \geq 0\pi^0\nu$	0.44± 0.08	0.59± 0.11	0.35± 0.09
Total	4.96±0.14	6.99± 0.22	2.20± 0.17

Table 5: Branching Ratio Measurements

$h^-\pi^0$ Selection I and $h^- \geq 2\pi^0$ Selection

$B_{h^-\pi^0}$	26.15 ±	0.38 (stat)	$^{+\ 0.51}_{-\ 0.80}$ (syst) %
$B_{h^-\geq 2\pi^0}$	9.90 ±	0.34 (stat)	± 0.57 (syst) %
$B_{h^-\pi^0} + B_{h^-> 2\pi^0}$	36.05 ±	0.35 (stat)	± 0.61 (syst) %

$h^-\pi^0$ Selection II and $h^- \geq 2\pi^0$ Selection

$B_{h^-\pi^0}$	26.25 ±	0.36 (stat)	± 0.52 (syst) %
$B_{h^-\geq 2\pi^0}$	9.89 ±	0.34 (stat)	± 0.55 (syst) %
$B_{h^-\pi^0} + B_{h^-> 2\pi^0}$	36.14 ±	0.33 (stat)	± 0.58 (syst) %

other branching ratios on the results are presented.

The systematic error due to "photon conversions" takes into account the uncertainty in the amount of material in the detector which leads to a slight difference in the modelled and observed number of photon conversions. The Monte Carlo indicates that 10% and 19% of the $h^-\pi^0$ and $h^- \geq 2\pi^0$ events have more than one good track. This is primarily due to photon conversions although about one-tenth is due to decays of π^0 into $e^+e^-\gamma$. Studies indicate that the data and Monte Carlo are in agreement on photon conversion to the level of 10%. Hence the uncertainty in the efficiencies due to photon conversions is estimated as 1% on the $h^-\pi^0$ efficiency and 2% on the $h^- \geq 2\pi^0$ efficiency, corresponding to an error on the branching ratios of 1% and 2% for $h^-\pi^0$ and $h^- \geq 2\pi^0$, respectively.

The "$x = p/E_{beam}$ requirement" systematic error gives the change in the branching ratio when the $x \geq 0.05$ requirement was removed from the $h^-\pi^0$ II and $h^- \geq 2\pi^0$ selections. This cut was implemented as there might be some uncertainty in the modelling of hadronic clusters from low momentum pions using the fine clustering algorithm. However the small effect of the cut on the results suggests that this is not a problem. Although this requirement was not applied to the $h^-\pi^0$ I selection, the solution of the linear equations yields a systematic uncertainty in the $h^-\pi^0$ branching ratio.

The "z-chamber requirement" systematic error gives the change in the branching ratio when the z drift chamber was included as part of the selection requirement. The OPAL jet chamber has excellent r-ϕ resolution but poorer z resolution. However the z-chamber, which improves the z resolution, was not required in the $h^-\pi^0$ II and $h^- \geq 2\pi^0$ selections due to its modest inefficiency. The $h^-\pi^0$ I selection required that there were z-chamber hits on all the charged tracks. Poor z resolution could affect the mass distributions. To estimate the size of this effect, the tracks were required to have hits from the z-chambers and the change in the branching ratio was included as a systematic uncertainty.

The "energy scale" systematic uncertainty includes: an energy scale error (the Monte Carlo energy scale is varied by $\pm 2\%$ at 1 GeV decreasing to $\pm 1\%$ at 45 GeV) which is due to the uncertainty of the calibration in the lead-glass calorimeter; an error in the energy correction for photons; and an error associated with the difference in energy resolution between the Monte Carlo and data. The large size of the error reflects the sensitivity of the measurement to the modelling of hadronic showers in the lead-glass calorimeter and the π^0 identification algorithms used.

The second half of the systematic errors arise from uncertainties in the non-τ and other τ backgrounds as well as uncertainties in the contributions of the $\pi^-3\pi^0$, K^* and other τ decay modes. The background from τ decays to the $e^-\overline{\nu}_e\nu_\tau$, $\mu^-\overline{\nu}_\mu\nu_\tau$, $h^-\nu_\tau$, $\pi^-K^0_L\nu_\tau$ + $\pi^-(K^0_S \to \pi^-\pi^+)\nu_\tau$ and $h^-h^+h^-(\geq 0\pi^0)\nu_\tau$ channels is relatively small and is insensitive to variations in the branching ratios of these channels within their errors. The error on the τ background includes the uncertainty on the efficiency due to Monte Carlo statistics and an uncertainty on the branching ratios of those channels.

The efficiencies for selecting $h^-\pi^0$ and $h^- \geq 2\pi^0$ decays depend on the relative branching ratios of the individual decays. The branching ratios of the $\tau^- \to K^{*-}\nu_\tau$ (and its subsequent decay products) and $\tau^- \to h^-3\pi^0\nu_\tau$ decays were independently varied by $\pm 100\%$ and the observed changes in the results were included as a systematic error.

Other τ decays that are not modelled may contribute to the $h^-\pi^0$ and $h^- \geq 2\pi^0$ samples. CLEO has published results on the $\tau^- \to \pi^-4\pi^0\nu_\tau$ branching ratio relative to the $\tau^- \to h^-\pi^0\nu_\tau$ branching ratio [14]. A branching ratio of 0.16% for the $\tau^- \to \pi^-4\pi^0\nu_\tau$ decay is obtained when the $h^-\pi^0$ branching ratio measured here is used. Included in this branching ratio is the

$\tau^- \to \eta\pi^-\pi^0\nu_\tau$ decay, also observed by CLEO [15], when the η decays into three π^0's . The $\tau^- \to \eta\pi^-\pi^0\nu_\tau$ decay has a branching ratio of $(0.17 \pm 0.02 \pm 0.02)\%$ [15]. The η can also decay into two photons approximately 39% of the time and could contribute to the signal. The $\tau^- \to \pi^-\omega\nu_\tau$ branching ratio has been measured by CLEO to be $(1.60 \pm 0.27 \pm 0.41)\%$ [15] and by ARGUS to be $(1.65 \pm 0.3 \pm 0.2)\%$ [16]. The ω can decay to a $\pi^0\gamma$ final state about 8.5% of the time, so the $\tau^- \to \pi^-\omega\nu_\tau$ branching ratio giving rise to only one charged track would be 0.14%. The efficiencies for detecting any of these decays were not determined, so their branching ratios are added as a systematic error to all three branching ratios.

CELLO has estimated the non-resonant $\tau^- \to \pi^-\pi^0\nu_\tau$ branching ratio to be $(0.3 \pm 0.1 \pm 0.3)\%$ based on a flat mass distribution [17]. To check for possible bias against non-resonant $\tau^- \to h^-\pi^0\nu_\tau$ decays, the efficiency for resonant $\tau^- \to h^-\pi^0\nu_\tau$ decays was studied as a function of the four-vector $h^-\pi^0$ mass. Assuming a flat mass distribution, the efficiency for detecting non-resonant $h^-\pi^0$ decays using selection I is 52% compared with 57% for resonant $h^-\pi^0$ decays. Since the efficiency for detecting non-resonant and resonant $h^-\pi^0$ decays is approximately equal, we assume that the $\tau^- \to h^-\pi^0\nu_\tau$ branching ratio quoted is the sum of the resonant and non-resonant components.

Although there is no error quoted explicitly for the uncertainty in the modelling of hadronic showers, it is included in a number of the errors listed in Table 6. The x-cut checks the modelling of low momentum hadrons. The energy scale variations are also sensitive to the shower modelling. The $h^-\pi^0$ selection I uses a shower shape technique for identifying particles and has a large uncertainty when the energy scale is varied. The $h^-\pi^0$ selection II and $h^- \geq 2\pi^0$ selection are much less sensitive to the shower shape. The limited cluster size means the tails of the showers, where the largest fluctuations may occur, are ignored. The two different methods for identifying particles should also be sensitive to any problems in the modelling of hadronic showers. The agreement between the methods suggests that systematic errors associated with the hadronic shower modelling are small and within the quoted systematic errors.

The measurements of the $B_{h^-\pi^0}$ and $B_{h^-\geq 2\pi^0}$ branching ratios are correlated to some extent. The correlation coefficient, ρ, is estimated from the statistical errors to be -0.53 and -0.58 when the $h^-\pi^0$ selection I and selection II were used. The small statistical error on the sum of the two branching ratios is a consequence of this correlation. The correlation coefficient for the systematic errors is estimated from the final systematic errors on $B_{h^-\pi^0}$, $B_{h^-\geq 2\pi^0}$ and $B_{h^-\pi^0} + B_{h^-\geq 2\pi^0}$. This is possible as the systematic error on $B_{h^-\pi^0} + B_{h^-\geq 2\pi^0}$ was evaluated independently. The correlation coefficient is estimated to be approximately -0.5 and -0.4 when the $h^-\pi^0$ selection I and $h^-\pi^0$ selection II are used, respectively.

The difference between the two sets of branching ratios given in Table 5 is small. As the two sets of results are not independent, they are not averaged. Instead we quote the branching ratio as determined by the $h^-\pi^0$ selection II and the $h^- \geq 2\pi^0$ selection as our "final result".

8 Discussion

The inclusive one-prong branching ratio can be compared with the sum of the exclusive one-prong branching ratios using these new results. OPAL has published τ branching ratio measurements for the $\tau^- \to e^-\bar{\nu}_e\nu_\tau$, $\tau^- \to \mu^-\bar{\nu}_\mu\nu_\tau$ and $\tau^- \to h^-\nu_\tau$ channels of $(17.4 \pm 0.5 \pm 0.4)\%$, $(16.8 \pm 0.5 \pm 0.4)\%$, and $(12.1 \pm 0.7 \pm 0.5)\%$, respectively [5]. The K^* contribution to the one-prong exclusive branching ratios is partly included in the $\tau^- \to h^-\pi^0\nu_\tau$ and $\tau^- \to h^- \geq 2\pi^0\nu_\tau$ branching ratios, however the $K^{*-} \to \pi^- K^0_L$ contribution is not. Assuming the Particle Data Group fit value for the branching ratio of $\tau^- \to K^{*-}\nu_\tau$ of $(1.42 \pm 0.18)\%$ [1], the $\tau^- \to \pi^- K^0_L\nu_\tau$

Table 6: Systematic uncertainties in the branching ratios

Description	$h^-\pi^0$ Selection I (%)	$h^- \geq 2\pi^0$ Selection (%)	$h^-\pi^0$ + $h^- \geq 2\pi^0$ (%)
Photon conversions	0.26	0.20	0.46
x requirement	0.09	0.19	0.10
z-chamber requirement	0.09	0.18	0.10
Energy Scale	0.65	0.43	0.22
Non-τ background	0.15	0.03	0.19
τ backgrounds	0.06	0.03	0.06
$\pi^\pm 3\pi^0$	0.33	0.23	0.11
K^{*-}	0.12	0.06	0.16
$h^\pm 4\pi^0$	0.16	0.16	0.16
$\pi^-\eta\pi^0$	0.07	0.07	0.07
$\pi^-\omega$	0.14	0.14	0.14
Total	$^{+0.51}_{-0.80}$	0.57	0.61

Description	$h^-\pi^0$ Selection II (%)	$h^- \geq 2\pi^0$ Selection (%)	$h^-\pi^0$ + $h^- \geq 2\pi^0$ (%)
Photon conversions	0.26	0.20	0.46
x requirement	0.22	0.21	0.01
z-chamber requirement	0.22	0.20	0.02
Energy Scale	0.21	0.41	0.20
Non-τ background	0.16	0.03	0.19
τ backgrounds	0.07	0.03	0.08
$\pi^\pm 3\pi^0$	0.26	0.22	0.04
K^{*-}	0.11	0.06	0.15
$h^\pm 4\pi^0$	0.16	0.16	0.16
$\pi^-\eta\pi^0$	0.07	0.07	0.07
$\pi^-\omega$	0.14	0.14	0.14
Total	0.52	0.55	0.58

branching ratio would be $(0.47 \pm 0.06)\%$ from isospin symmetry arguments. In addition, the $\tau^- \to \pi^- \mathrm{K}^0_S \nu_\tau \to \pi^-\pi^+\pi^-\nu_\tau$ decay, with a branching ratio of $(0.33 \pm 0.04)\%$, is also considered a one-prong decay in the inclusive measurement. Including these K^* channels, the sum of the exclusive one-prong OPAL branching ratios would give $(83.3 \pm 1.4)\%$ consistent with the measured OPAL inclusive one-prong branching ratio of $(84.48 \pm 0.27 \pm 0.23)\%$ [6].

The OPAL τ branching ratios indicate that there is no one-prong problem. Similarly, ALEPH [2] and CELLO [3] report no inconsistency between their one-prong exclusive and inclusive branching ratio measurements. However OPAL's solution to the one-prong problem is different from both ALEPH and CELLO, with a higher fraction of $\tau^- \to \mathrm{h}^-\pi^0\nu_\tau$ decays and a smaller fraction of $\tau^- \to \mathrm{h}^- \geq 2\pi^0\nu_\tau$ decays in the one-prong sample.

The branching ratio of the $\tau^- \to \mathrm{h}^- \geq 1\pi^0\nu_\tau$ decay is measured to be $(36.14 \pm 0.33 \pm 0.58)\%$. This branching ratio was calculated by adding the $\tau^- \to \mathrm{h}^-\pi^0\nu_\tau$ and $\tau^- \to \mathrm{h}^- \geq 2\pi^0\nu_\tau$ branching ratios. The results presented here are in good agreement with the ALEPH [2] and CELLO [3] results of $(37.08 \pm 1.62)\%$ and $(36.6 \pm 2.1)\%$ respectively. The ALEPH result was obtained by adding their $\tau^- \to \mathrm{h}^-\pi^0\nu_\tau$, $\tau^- \to \mathrm{h}^-2\pi^0\nu_\tau$ and $\tau^- \to \mathrm{h}^- \geq 3\pi^0\nu_\tau$ branching ratios. The CELLO result was obtained by adding their $\tau^- \to \mathrm{h}^-2\gamma\nu_\tau$ and $\tau^- \to \mathrm{h}^- > 2\gamma\nu_\tau$ branching ratios.

The branching ratio of the $\tau^- \to \mathrm{h}^-\pi^0\nu_\tau$ decay is measured to be $(26.25 \pm 0.36 \pm 0.52)\%$ and is compared with other published branching ratios in Figure 4. The branching ratios indicated by a $(*)$ have been published as either $\tau^- \to \rho^-\nu_\tau$ or $\tau^- \to \pi^-\pi^0\nu_\tau$, and 0.5% has been added to them to account for the $\mathrm{K}^-\pi^0$ contribution. The $\tau^- \to \mathrm{h}^-\pi^0\nu_\tau$ branching ratio measured here is high when compared with the Particle Data Group average value $(23.8\pm 0.8)\%$ and fit value $(24.4\pm0.6)\%$ [1], but it is consistent with most measurements.

Kuhn and Santamaria [23] predict that $\Gamma(\tau^- \to \pi^-\pi^0\nu_\tau)/\Gamma(\tau^- \to \mathrm{e}^-\bar{\nu}_\mathrm{e}\nu_\tau) = 1.32 \pm 0.05$ on the assumption that the Conserved Vector Current (CVC) principle is correct. Using OPAL's branching ratio for $\tau^- \to \mathrm{e}^-\bar{\nu}_\mathrm{e}\nu_\tau$ of $(17.4 \pm 0.5 \pm 0.4)\%$ [5] and the $\tau^- \to \mathrm{h}^-\pi^0\nu_\tau$ branching ratio measured here, one obtains $\Gamma(\tau^- \to \pi^-\pi^0\nu_\tau)/\Gamma(\tau^- \to \mathrm{e}^-\bar{\nu}_\mathrm{e}\nu_\tau) = 1.48 \pm 0.07$. The $\tau^- \to \mathrm{K}^-\pi^0\nu_\tau$ branching ratio of $(0.47 \pm 0.06)\%$ was subtracted from the $\tau^- \to \mathrm{h}^-\pi^0\nu_\tau$ branching ratio to give the $\tau^- \to \pi^-\pi^0\nu_\tau$ branching ratio. The result measured here is consistent (within two standard deviations) with the CVC prediction.

The branching ratio of the $\tau^- \to \mathrm{h}^- \geq 2\pi^0\nu_\tau$ decay was measured to be $(9.89\pm0.34\pm0.55)\%$ and is compared with other published branching ratios in Figure 5. The ALEPH[2] and CELLO [17] branching ratios were calculated by adding their $\tau^- \to \mathrm{h}^-2\pi^0\nu_\tau$ and $\tau^- \to \mathrm{h}^- \geq 3\pi^0\nu_\tau$ branching ratios. CLEO has measured the branching ratios of the $\tau^- \to \mathrm{h}^-2\pi^0\nu_\tau$, $\tau^- \to \mathrm{h}^-3\pi^0\nu_\tau$ and $\tau^- \to \mathrm{h}^-4\pi^0\nu_\tau$ decays relative to the $\tau^- \to \mathrm{h}^-\pi^0\nu_\tau$ branching ratio [14]. In Figure 5 the sum of the CLEO branching ratios is plotted using both our $\tau^- \to \mathrm{h}^-\pi^0\nu_\tau$ branching ratio and the Particle Data Group fit value. Our result for the $\tau^- \to \mathrm{h}^- \geq 2\pi^0\nu_\tau$ branching ratio is consistent with previous individual measurements. However it is significantly lower than the Particle Data Group average value $(13.7\pm1.1)\%$ and fit value $(13.2\pm0.7)\%$ for the $\tau^- \to \mathrm{h}^- \geq 2\pi^0\nu_\tau$ channel, but in good agreement with the sum of the average values for the $\tau^- \to \mathrm{h}^-2\pi^0\nu_\tau$ and $\tau^- \to \mathrm{h}^- \geq 3\pi^0\nu_\tau$ channels $(10.8\pm0.9)\%$ [1].

9 Conclusions

The branching ratio of the $\tau^- \to \mathrm{h}^-\pi^0\nu_\tau$ and $\tau^- \to \mathrm{h}^- \geq 2\pi^0\nu_\tau$ decays have been measured with the OPAL detector at LEP. The branching ratios are

$$
\begin{aligned}
B_{h\pi^0} &= (26.25 \pm 0.36 \pm 0.52)\% \\
B_{h\geq 2\pi^0} &= (9.89 \pm 0.34 \pm 0.55)\% \\
B_{h\pi^0} + B_{h\geq 2\pi^0} &= (36.14 \pm 0.33 \pm 0.58)\%
\end{aligned}
$$

where the first error is statistical and the second error is systematic.

The sum of the $\tau^- \to \mathrm{h}^-\pi^0\nu_\tau$ and $\tau^- \to \mathrm{h}^- \geq 2\pi^0\nu_\tau$ branching ratios gives a $\tau^- \to \mathrm{h}^- \geq 1\pi^0\nu_\tau$ branching ratio that is the most precise measurement to date and is in agreement with previous measurements. The results, when added together with previously published OPAL one-prong measurements, show that the exclusive one-prong branching ratio is consistent with the inclusive one-prong branching ratio.

The measurements of the $\tau^- \to \mathrm{h}^-\pi^0\nu_\tau$ and $\tau^- \to \mathrm{h}^- \geq 2\pi^0\nu_\tau$ branching ratios have precision comparable or better than previous measurements. The $\tau^- \to \mathrm{h}^-\pi^0\nu_\tau$ branching ratio is higher than but consistent with published branching ratios, while the $\tau^- \to \mathrm{h}^- \geq 2\pi^0\nu_\tau$ branching ratio is lower than but consistent with previous measurements.

Acknowledgements

It is a pleasure to thank the SL Division for the efficient operation of the LEP accelerator, the precise information on the absolute energy, and their continuing close cooperation with our experimental group. In addition to the support staff at our own institutions we are pleased to acknowledge the
Department of Energy, USA,
National Science Foundation, USA,
Texas National Research Laboratory Commission, USA,
Science and Engineering Research Council, UK,
Natural Sciences and Engineering Research Council, Canada,
Fussefeld Foundation,
Israeli Ministry of Energy and Ministry of Science,
Minerva Gesellschaft,
Japanese Ministry of Education, Science and Culture (the Monbusho) and a grant under the Monbusho International Science Research Program,
German Israeli Bi-national Science Foundation (GIF),
Direction des Sciences de la Matière du Commissariat à l'Energie Atomique, France,
Bundesministerium für Forschung und Technologie, Germany,
National Research Council of Canada,
A.P. Sloan Foundation and Junta Nacional de Investigação Científica e Tecnológica, Portugal.

References

[1] Particle Data Group, K. Hikasa *et al.*, Phys. Rev. **D45** (1992) 1 and references therein.

[2] ALEPH Collaboration, D. Decamp *et al.*, Z. Phys. **C54** (1992) 211.

[3] CELLO Collaboration, H.J. Behrend *et al.*, Z. Phys. **C46** (1990) 537.

[4] OPAL Collaboration, K. Ahmet *et al.*, Nucl. Instr. and Meth. **A305** (1991) 275.

[5] OPAL Collaboration, G. Alexander *et al.*, Phys. Lett. **B266** (1991) 201.

[6] OPAL Collaboration, P. Acton *et al.*, Phys. Lett. **B288** (1992) 373.

[7] OPAL Collaboration, G. Alexander *et al.*, Z. Phys. **C52** (1991) 175.

[8] M. Böhm, A. Denner and W. Hollik, Nucl. Phys. **B304** (1988) 687;
F.A. Berends, R. Kleiss, W. Hollik, Nucl. Phys. **B304** (1988) 712; BABAMC.

[9] S. Jadach, J.H. Kühn, and Z. Was, Comp. Phys. Comm. **64** (1991) 275;
TAUOLA Version 1.5.
S. Jadach, B.F.L. Ward, and Z. Was, Comp. Phys. Comm. **66** (1991) 276;
KORALZ, Version 3.8.

[10] T. Sjöstrand, Comp. Phys. Comm. 39 (1986) 347; JETSET Version 7.3.

[11] R. Bhattacharya, J. Smith, G. Grammer, Phys. Rev. **D15** (1977) 3267;
J. Smith, J.A.M. Vermaseren, G. Grammer, Phys. Rev. **D15** (1977) 3280.

[12] J. Allison *et al.*, Nucl. Instr. and Meth. **A317** (1992) 47.

[13] A. Rougé, "Tau Decays as Polarization Analyzers", Proceedings of the Workshop on Tau Lepton Physics, 24-27 September 1990, eds. M. Davier and B. Jean-Marie, Orsay, France.

[14] CLEO Collaboration, M. Procario *et al.*, Phys. Rev. Lett. **70** (1993) 1207.

[15] CLEO Collaboration, M. Artuso *et al.*, Phys. Rev. Lett. **69** (1992) 3278.

[16] ARGUS Collaboration, H. Albrecht *et al.*, Z. Phys. **C41** (1988) 405.

[17] CELLO Collaboration, H.J. Behrend *et al.*, Z. Phys. **C23** (1984) 103.

[18] ARGUS Collaboration, H. Albrecht *et al.*, Z. Phys. **C56** (1992) 339.

[19] DELPHI Collaboration, P. Abreu *et al.*, Z. Phys. **C55** (1992) 555.

[20] Crystal Ball Collaboration, D. Antreasyan *et al.*, Phys. Lett. **259** (1991) 216.

[21] Mark III Collaboration, J. Adler *et al.*, Phys. Rev. Lett. **59** (1987) 1527.

[22] Mark II Collaboration, J.M. Yelton *et al.*, Phys. Rev. Lett. **56** (1986) 812.

[23] J.H. Kühn and A. Santamaria, Z. Phys. **C48** (1990) 445.

[24] Mark II Collaboration, P. R. Burchat *et al.*, Phys. Rev. **D35** (1987) 27.

[25] TPC Collaboration, H. Aihara *et al.*, Phys. Rev. Lett. **57** (1986) 1836.

Figure Captions

Figure 1 The mass of (a) the two photons and (b) the jet for decays that pass the $h^-\pi^0$ selection I. The data are represented by the points on the plot. The Monte Carlo prediction is divided into three parts: the unshaded part is the $h^-\pi^0$ decays, the diagonal cross hatch part is the $h^- \geq 2\pi^0$ decays and the double cross hatched part is the background from other τ decays. The arrows indicate the positions of the mass cuts applied.

Figure 2 The mass of the jet for decays that pass (a) the $h^-\pi^0$ selection II and (b) the $h^- \geq 2\pi^0$ selection. The data are represented by the points on the plot. The Monte Carlo prediction is divided into three parts: for the upper plot the unshaded part is the $h^-\pi^0$ decays, the diagonal cross hatch part is the $h^- \geq 2\pi^0$ decays and the double cross hatched part is the background from other τ decays. For the lower plot the unshaded part is the $h^- \geq 2\pi^0$ decays, the diagonal cross hatch part is the $h^-\pi^0$ decays and the double cross hatched part is the background from other τ decays. The arrows indicate the positions of the mass cuts applied.

Figure 3 The mass of the neutral clusters for jets with only two neutral clusters. The upper plot (a) is for decays that pass the $h^-\pi^0$ selection II. The arrow indicates the position of the mass cut applied. The lower plot (b) uses the π^0 finding algorithm employed in the $h^- \geq 2\pi^0$ selection. The lower plot demonstrates that π^0's are reconstructed with the π^0 finding algorithm. Note that the cuts applied to the data to generate the lower plot differ from those applied in the $h^- \geq 2\pi^0$ selection. For both plots, the data are represented by the points on the plot; and the Monte Carlo prediction is divided into three parts: the unshaded part is the $h^-\pi^0$ decays, the diagonal cross hatch part is the $h^- \geq 2\pi^0$ decays and the doubly cross hatched part is the background from other τ decays.

Figure 4 The published branching ratios for the $\tau^- \to h^-\pi^0\nu_\tau$ decays are shown. The branching ratios labelled with a $(*)$ are published as either $\tau^- \to \rho^-\nu_\tau$ or $\tau^- \to \pi^-\pi^0\nu_\tau$ and have been corrected for $K^-\pi^0$ contributions.

Figure 5 The published branching ratios for the $\tau^- \to h^- \geq 2\pi^0\nu_\tau$ decay are shown. The branching ratios labelled with a (Σ) have been determined by summing up the $\tau^- \to h^-2\pi^0\nu_\tau$, $\tau^- \to h^-3\pi^0\nu_\tau$ and $\tau^- \to h^-4\pi^0\nu_\tau$ contributions. The CLEO $\tau^- \to h^- \geq 2\pi^0\nu_\tau$ branching ratio is dependent on the $\tau^- \to h^-\pi^0\nu_\tau$ branching ratio. Two numbers for CLEO are given, one is based on the $\tau^- \to h^-\pi^0\nu_\tau$ branching ratio measured here and the other on the Particle Data Group branching ratio.

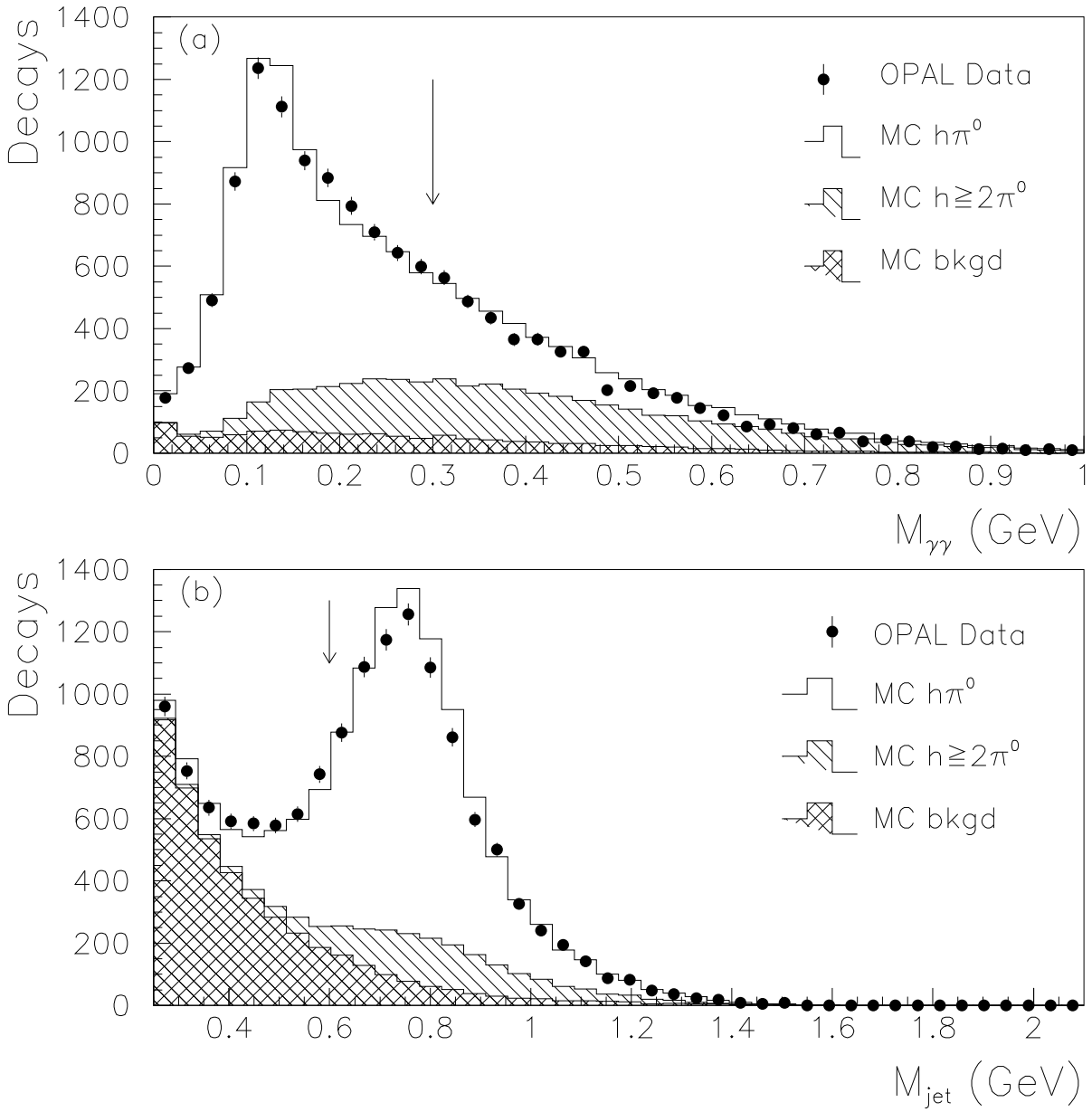
(a)
Decays
1400
1200
1000
800
600
400
200
0
0
0.1
0.2
0.3
0.4
0.5
0.6
0.7
0.8
0.9
1
OPAL Data
MC hπ⁰
MC h≧2π⁰
MC bkgd
Mγγ (GeV)
(b)
Decays
1400
1200
1000
800
600
400
200
0
0.4
0.6
0.8
1
1.2
1.4
1.6
1.8
2
OPAL Data
MC hπ⁰
MC h≧2π⁰
MC bkgd
Mjet (GeV)

Figure 1

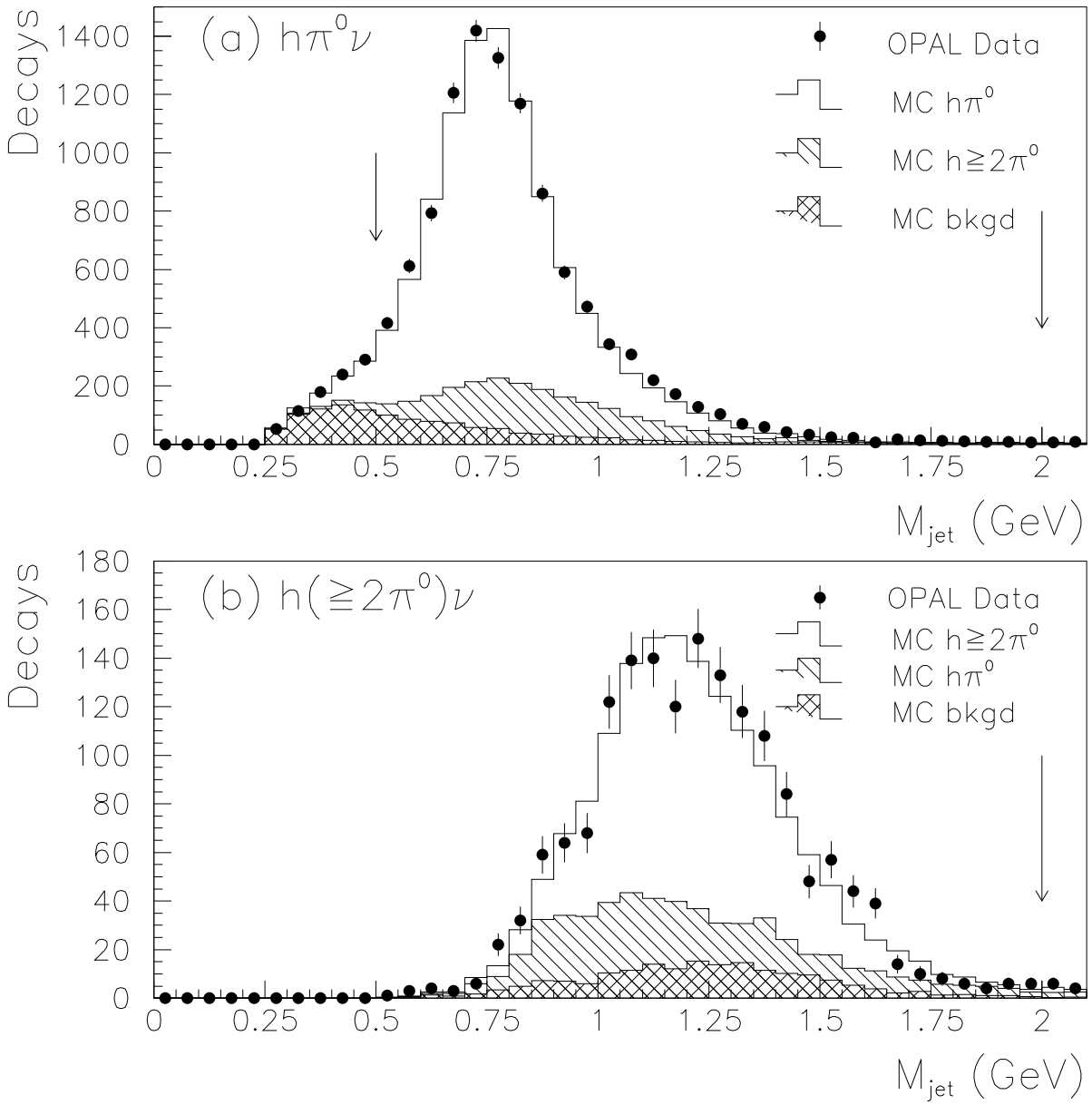
(a) hπ⁰ν
OPAL Data
MC hπ⁰
MC h≧2π⁰
MC bkgd
Decays
M_jet (GeV)
(b) h(≧2π⁰)ν
OPAL Data
MC h≧2π⁰
MC hπ⁰
MC bkgd
Decays
M_jet (GeV)

Figure 2

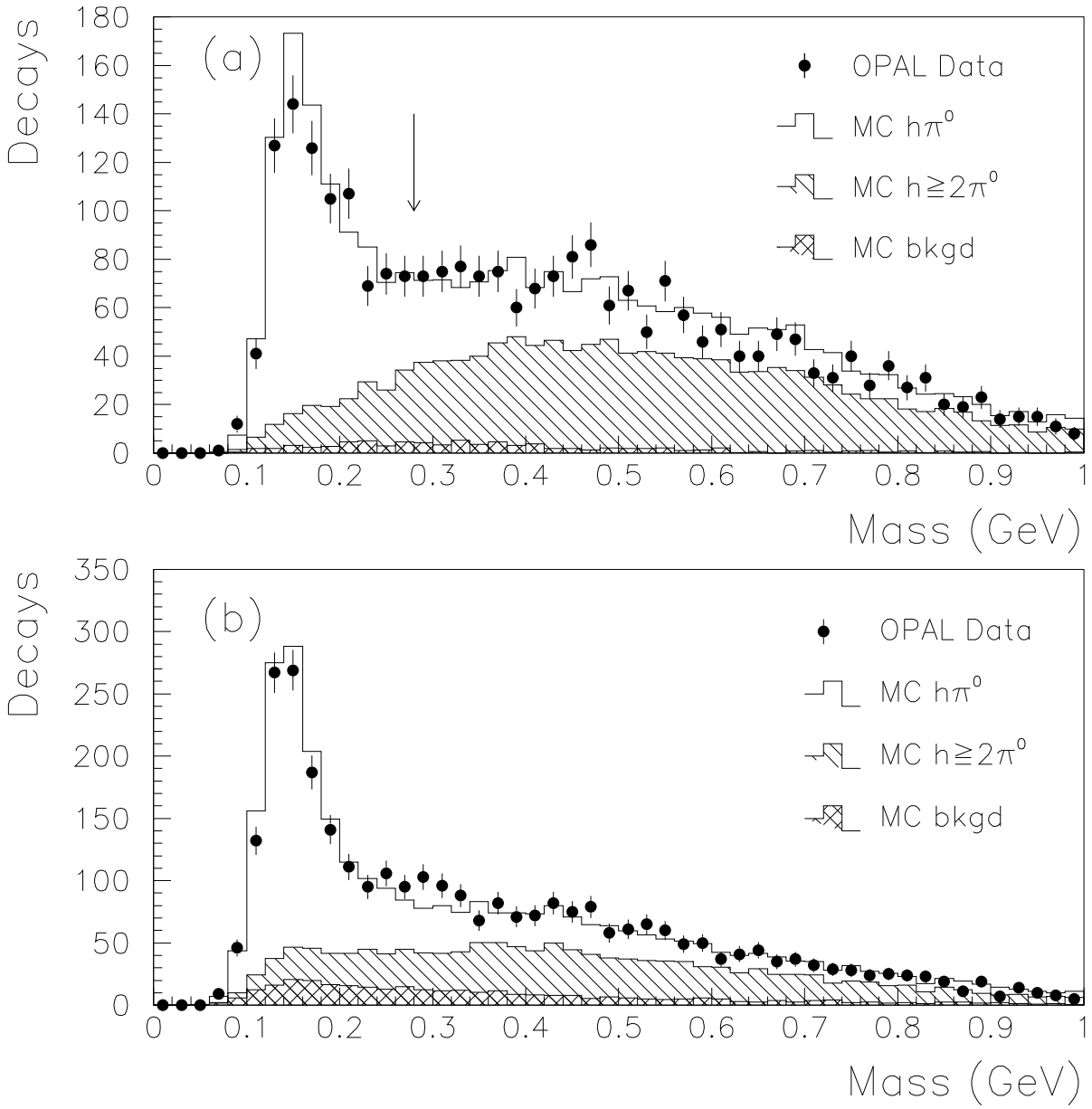
(a)
Decays
OPAL Data
MC hπ⁰
MC h≧2π⁰
MC bkgd
Mass (GeV)
(b)
Decays
OPAL Data
MC hπ⁰
MC h≧2π⁰
MC bkgd
Mass (GeV)

Figure 3

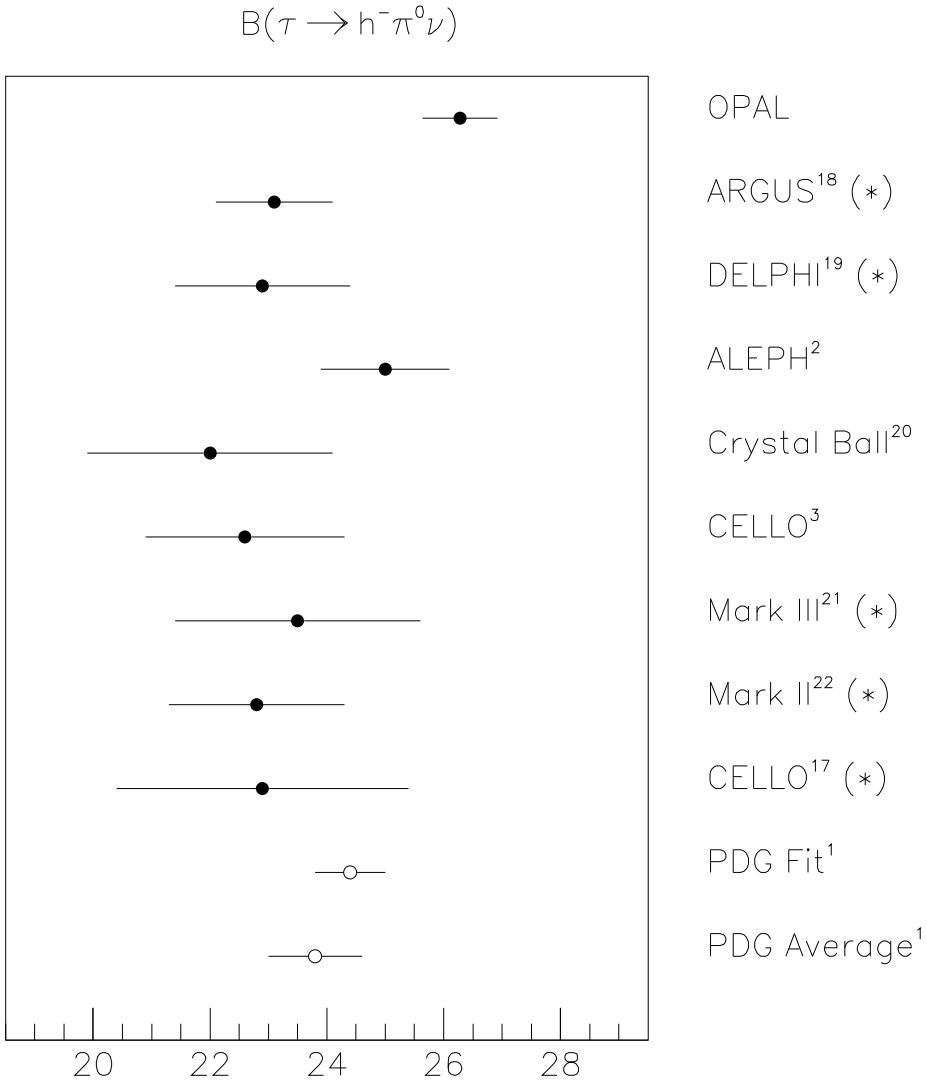
B(τ → h⁻π⁰ν)
OPAL
ARGUS[18] (*)
DELPHI[19] (*)
ALEPH[2]
Crystal Ball[20]
CELLO[3]
Mark III[21] (*)
Mark II[22] (*)
CELLO[17] (*)
PDG Fit[1]
PDG Average[1]
20
22
24
26
28

Figure 4

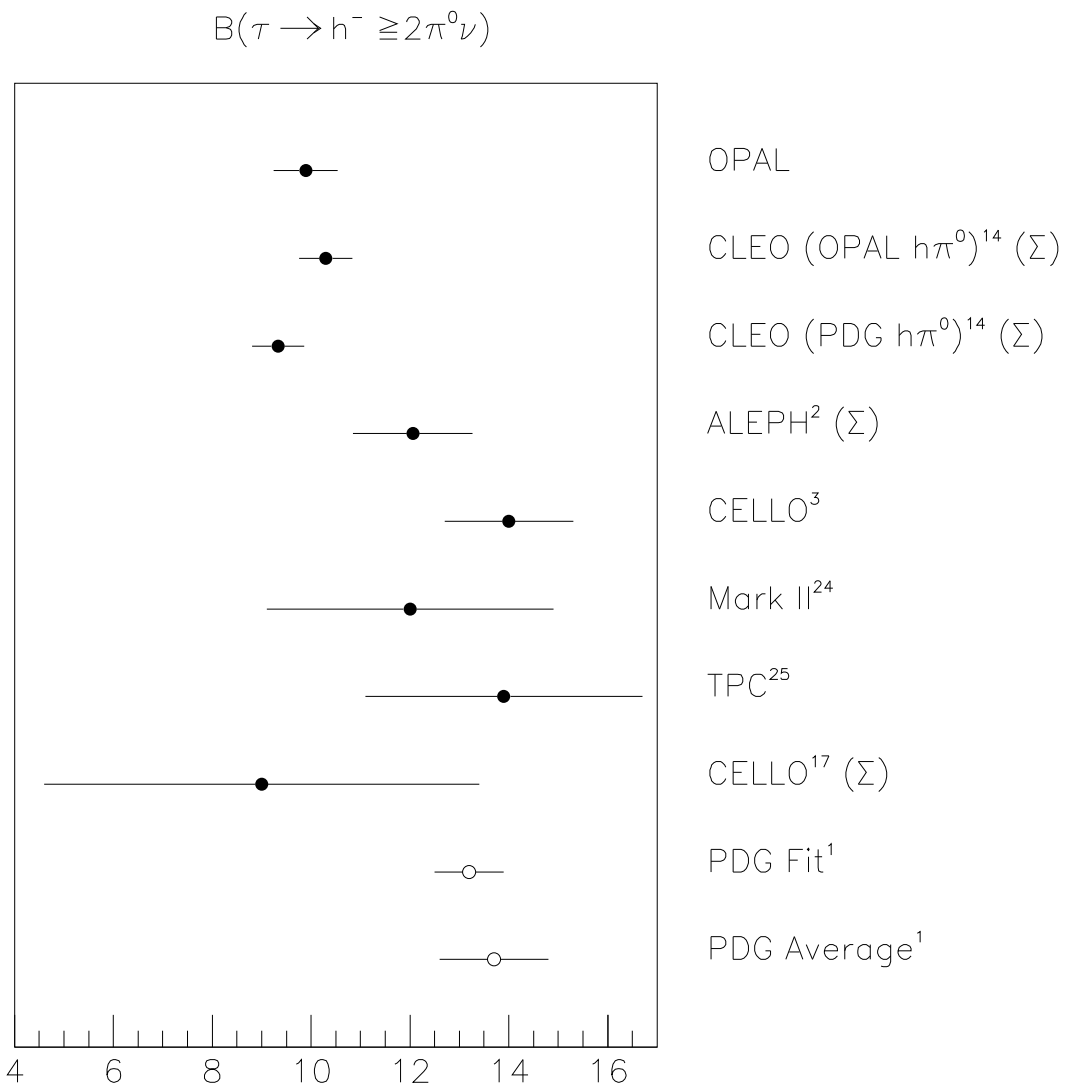
B(τ → h⁻ ≧2π⁰ν)
OPAL
CLEO (OPAL hπ⁰)[14] (Σ)
CLEO (PDG hπ⁰)[14] (Σ)
ALEPH[2] (Σ)
CELLO[3]
Mark II[24]
TPC[25]
CELLO[17] (Σ)
PDG Fit[1]
PDG Average[1]
4
6
8
10
12
14
16

Figure 5